Structural Engineering and Mechanics, *Vol. 50, No. 4 (2014) 501-524*
DOI: http://dx.doi.org/10.12989/sem.2014.50.4.501

Loading capacity evaluation of composite box girder with corrugated webs and steel tube slab

Jun He[1a], Yuqing Liu[*2], Xiaoqing Xu[2b] and Laibin Li[3]

[1]*School of Civil Engineering and Architecture, Changsha University of Science & Technology, Hunan, China*
[2]*Department of Bridge Engineering, Tongji University, Shanghai, China*
[3]*Xingtai Road & Bridge Construction Corporation, Hebei, China*

(Received September 13, 2012, Revised September 3, 2013, Accepted March 20, 2014)

Abstract. This paper presents a type of composite box girder with corrugated webs and concrete filled steel tube slab to overcome cracking on the web and reduce self-weight. Utilizing corrugated steel web improves the efficiency of prestressing introduced into the top and bottom slabs due to the accordion effect. In order to understand the loading capacity of such new composite structure, experimental and numerical analyses were conducted. A full-scale model was loaded monotonically to investigate the deflection, strain distribution, loading capacity and stiffness during the whole process. The experimental results show that test specimen has enough loading capacity and ductility. Based on experimental works, a finite element (FE) model was established. The load-displacement curves and stress distribution predicted by FE model agree well with that obtained from experiments, which demonstrates the accuracy of proposed FE model. Moreover, simplified theoretical analysis was conducted depending on the assumptions which were confirmed by the experimental and numerical results. The simplified analysis results are identical with the tested and numerical results, which indicate that simplified analytical model can be used to predict the loading capacity of such composite girder accurately. All the findings of present study may provide reference for the application of such structure in bridge construction.

Keywords: composite girder; corrugated steel web; steel tube slab; loading capacity; finite element analysis; simplified analytical model

1. Introduction

Bridges with short or medium span are common in practice and have been mostly built in the past adopting reinforced or prestressed concrete solutions. It was confirmed that reinforced concrete structures may have problems such as excessive cracking and heavy self-weight, making it difficult to achieve long spans. Composite solutions which can sufficiently offer the advantages of both reinforced concrete and steel have been promoted and researched to solve these problems (Brozzetti 2000, Nakamura *et al.* 2002), especially the prestressed composite members (Ayyub *et al.* 1992a, b, Chen and Gu 2005).

∗Corresponding author, Professor, E-mail: yql@tongji.edu.cn
[a]Associate Professor, E-mail: frankhejun@gmail.com
[b]Ph.D. Student, E-mail: xiaoqing.xu.china@gmail.com

http://www.techno-press.org/?journal=sem&subpage=8 ISSN: 1225-4568 (Print), 1598-6217 (Online)

Typical steel beams have huge axial rigidity on their section, which result in low effective prestress. In addition, excessive stiffeners should be arranged to prevent buckling instability. To overcome such limitations with existing prestressed composite members, the advantages of using corrugated steel webs along with external prestressing for box or I-girder composite systems in bridge construction were recognized by Campenon Bernard BTP, France (Cheyrezy and Combault 1990). The first highway bridge using corrugated webs was the Cognac Bridge, built in France as an experimental bridge in 1986. Such bridges in French inspired a number of similar structures in Japan, Germany, USA, China and other countries. Based on the promising new type hybrid structure, their flexural behavior (Mo *et al*. 2003), shear behavior (Sause and Braxtan 2011) and torsional behavior (Mo and Fan 2006) had been experimentally and numerically investigated. Moreover, the fatigue life of steel bridge I-girders with trapezoidal web corrugations was studied and large-scale test girders were experimented (Sause *et al.* 2006, Ibrahim *et al.* 2006). In order to improve the structural performance of continuous girders with corrugated webs under hogging moment, He *et al*. (2012a, b, 2014) proposed and analyzed partially encased composite girders with corrugated steel webs.

The performance of composite girders depends largely on an effectiveness of shear connection at the interface between concrete and steel. Corrugated steel webs have very low axial rigidity, which requires relatively flexible shear connectors. Shear connectors without using a top steel flange was proposed, and no top steel flange may improve cost performance of composite girders with corrugated steel webs (Kosa *et al.* 2006). With the purpose of providing the theoretical foundation and playing an important role in the development of composite bridges with corrugated steel webs, the authors summarized the state-of-the-art report on analysis, design and construction of such composite bridges related to some important references (He *et al.* 2012c).

This paper presents a type of composite box girder with corrugated webs and steel tube slab, as shown in Fig. 1. Prestress is efficiently introduced to the slabs due to the low axial rigidity of corrugated webs. In addition, steel tube is filled with concrete for the sake of prestressing introduction and avoiding the buckling of thin-walled steel tube. The corrugated steel webs are connected to both top and bottom slabs by welding, no additional connectors are required. All the steel structural components are fabricated and assembled in the factory with good quality and high efficiency. The box girders are then transported to the construction field, and connected by the steel diaphragms to meet the requirement of bridge deck width, finally concrete are directly casted on the top steel plate and connected to the steel plate through the bent-up bars and reinforcing bars, no formworks or supporting posts are necessary for the deck, which leads to save construction time and cost.

In order to understand the mechanical behavior and loading capacity of such new composite structure, experimental and numerical analyses were conducted. Firstly, a full-scale model of composite box girder with corrugated steel webs was loaded monotonically to investigate the deflection, strain distribution, and loading capacity during the whole process. On the basis of experimental works, a FE model was established. Additionally, the numerical results were compared to the experimental ones in order to verify the proposed FE model and reveal some mechanical characteristics of such composite structure. Moreover, simplified theoretical analyses were conducted depending on the assumptions which were confirmed by the experimental and numerical results, such as the plane section assumption of bending strain on slabs, uniformly distribution of shear strain along the web height, and perfect connection between steel plate and concrete slab. All the findings of experimental and analytical works at present study may provide reference for the application of such structure in bridge construction.

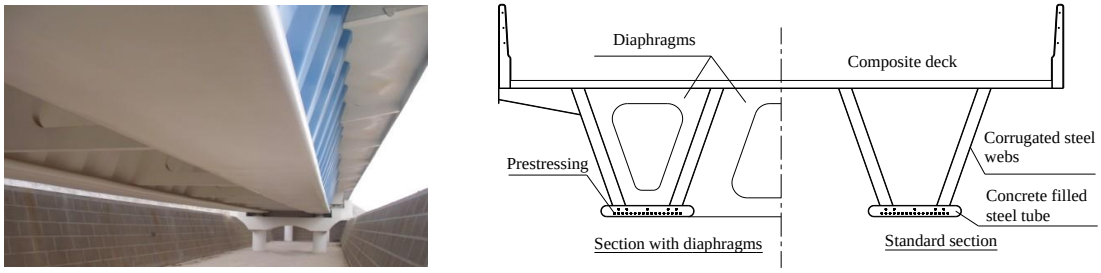

(a) Bridge application (b) Cross section

Fig. 1 Composite box girder bridge with corrugated webs and steel tube slab

2. Experimental program

2.1 Test specimen

A full-scale composite box girder with corrugated webs and steel tube slab was prepared and tested to investigate the load carrying capacity, as shown in Fig. 2. The total length and height of the specimen are 30 m and 1.8 m respectively. The top deck and bottom slab adopt steel-concrete composite structures. The width and thickness of the top deck are 3.5 m and 0.1m respectively, and one layer reinforcing bars with diameter of 10mm and spacing of 10cm are embedded in the concrete deck. While the width and thickness of the bottom concrete filled steel tube slab are 1.22 m and 0.15 m respectively, and two layers (5 bundles in the upper layer, 17 bundles in the bottom layer) prestressed steel tendons ($7\phi5$) are installed in the bottom slab. Self-compacting concrete (a highly flowable, non-segregating concrete) was filled into steel tube slab without any mechanical vibration to improve the constructability and quality of infill concrete. Also, some air-bleed holes were opened and checked during concrete filling process to avoid voids occurrence. Corrugated steel plates are used for the webs, the unit wavelength is 1000 mm, the width of horizontal and inclined plate are 340 mm and 226 mm respectively, the projected width of inclined plate is 160 mm, and the details of the dimensions for the corrugated web are depicted in Fig. 2(c). The thickness of corrugated steel webs, steel plates of the top deck and the bottom tube is 6 mm. The steel components of test specimen were fabricated and assembled in the factory. The bent-up bars and reinforcing bars were welded and arranged on the steel top plate to connect the concrete. Concrete were then poured on the steel plate to become composite deck without requiring formworks or supporting posts. The fabrication process is shown in Fig. 3.

2.2 Material properties

Concrete with a design compressive strength of 40N/mm^2 is used. The average compressive strength, tensile strength and Young's modulus of three cube specimens at 28 days after concrete casting are 39.1 MPa, 2.45 MPa and 3.28×10^4 MPa. The characteristic tensile strength is used in prediction of the cracking resistance of the specimens. The steel components are made of weathering steel Q355qENH with tensile yielding stress of 410 MPa and ultimate stress of 540 MPa, and reinforcements adopt steel HRB335 with nominal tensile yielding stress of 335 MPa. The ultimate tensile strength and Young's modulus of prestressing steel strands are 1860 MPa and 1.95×10^5 MPa respectively.

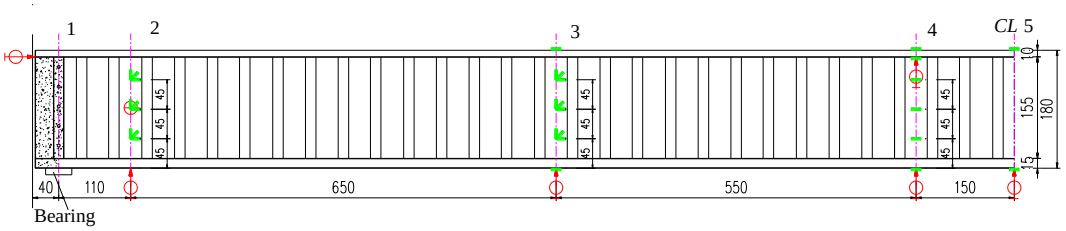

(a) Elevation view, cm

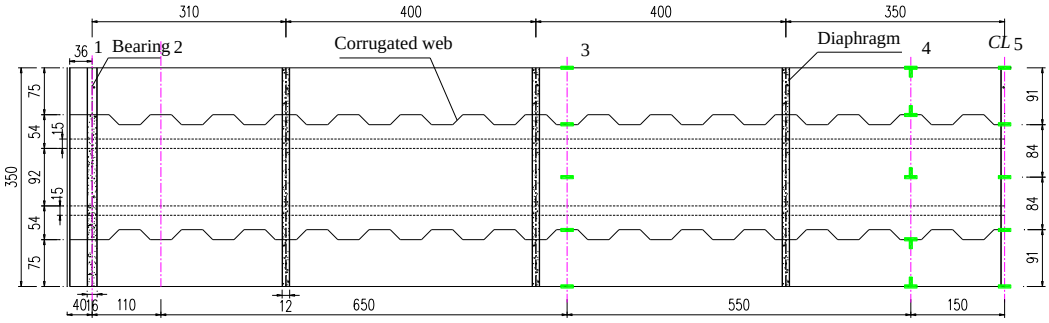

(b) Plan view, cm

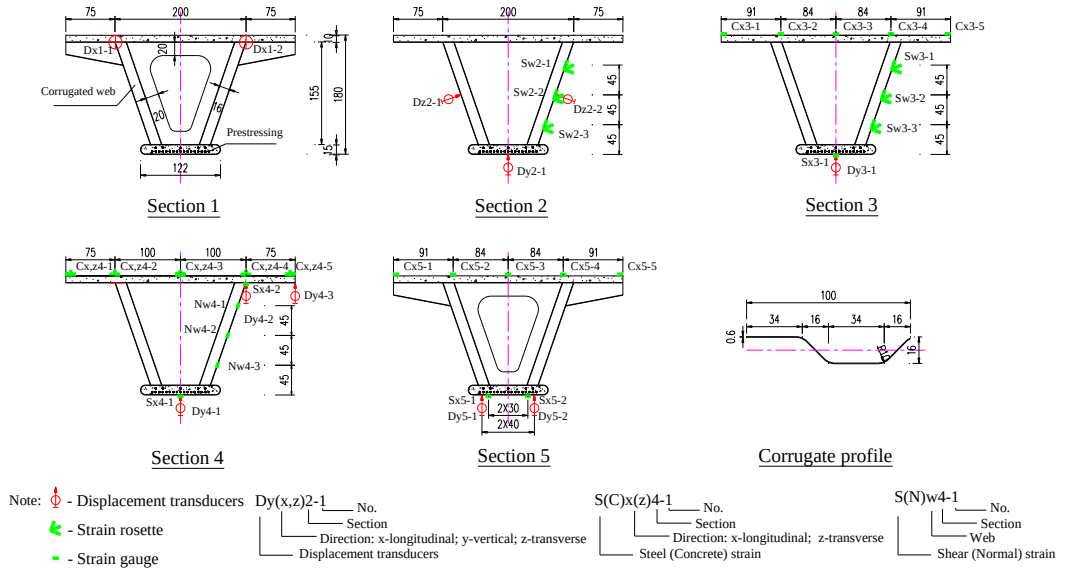

(c) Cross-section view, cm

Fig. 2 Test specimen and instruments of composite box girder with corrugated webs

2.3 Loading and measurements

Load carrying capacity test of composite box girder was carried out on bridge construction site. The tested composite box girder was simply supported by the bearings, and the partially-uniform

(a) Steel box-girder

(b) Steel tube after prestressing introduced

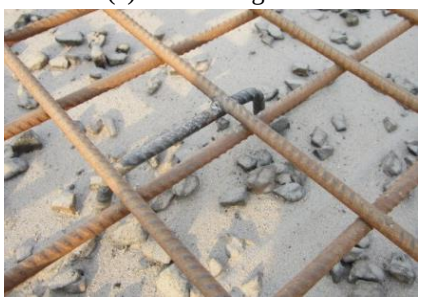

(c) Arrangement of reinforcing bars at top deck

(d) Composite box girder after concrete casting

Fig. 3 Fabrication process of test specimen

distributed load was applied on the deck using steel blocks. Each steel block has the length of 9.3 m and weight of 1.64 ton, and the section of the steel block is square shape (15 cm×15 cm). The steel blocks were piled up in three zones along the axial direction, the distance between two adjacent zones is 80 cm, the length and width of each zone are 9.3 m and 2.5 m respectively, which can place about 15 pieces in one layer along lateral direction. In order to apply the distributed load more uniformly and reduce the constraint of curvature deformation for test specimen by steel blocks, sand cushion with the thickness about 20cm was put on the top deck before steel blocks were piled up. Three cranes lifted and placed the steel stocks on the determined location of three zones at the same time. The crane lifted 3 pieces of steel blocks every time, thus each layer should be placed five times, and the steel blocks were piled up from the middle to the edge of the section. The first layer of the steel blocks was applied as preloading stage to check the good contact between the support and loading equipment, the reliability of all the test equipment and the workability of all measurement instruments. The loading was increased up to the yielding of the bottom steel tube (>500 ton). The height of steel blocks was more than 2 m, which was higher than that of the girder. It was dangerous to pile up more steel stocks although six lateral supports were installed to prevent steel blocks falling down. Therefore the loading test stopped after the stage of bottom steel tube yielding. Fig. 4 shows the test set-up and loading procedure.

Displacement transducers LVDTs (Linear Variable Differential Transformer) were used to measure the vertical deflection at the mid-span and 1/4 span of the girder, as shown in Fig. 1(a). LVDTs were also installed to measure the lateral displacements at the steel web near the supporting section (Sec.2). In addition, LVDTs were installed at end section (Sec.1) to measure the relative displacement (slip) between the steel girder and concrete slab. At critical sections, such as the middle section (Sec.5), the strains were measured using 50mm electrical gauges for the concrete and 5 mm electrical gauges for the steel plate, strain rosette were installed on steel web to

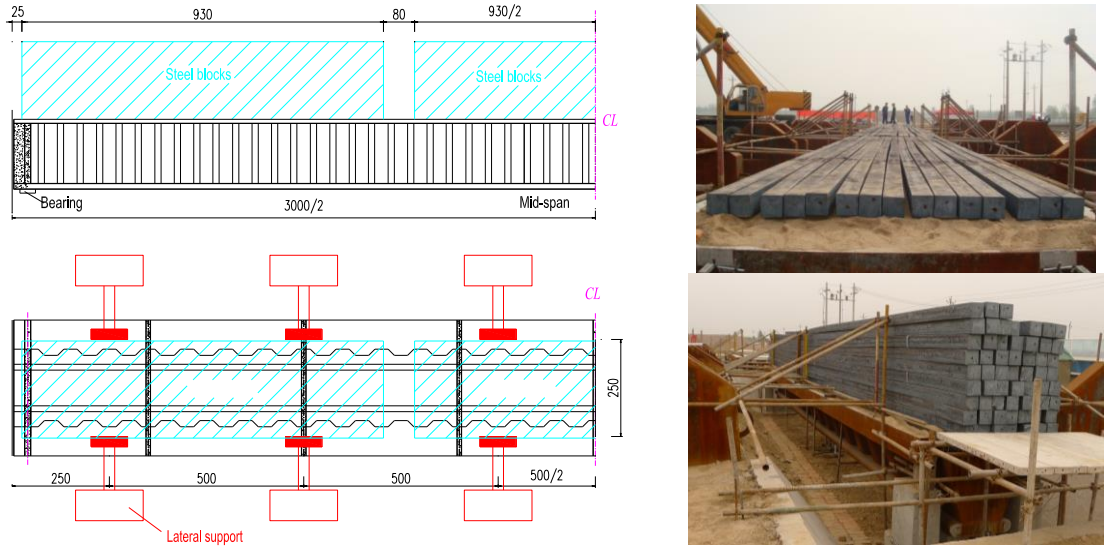

Fig. 4 Test set-up and loading procedure, cm

obtain the shear strain, the arrangement of strain gauges and LVDTs is shown in Fig. 2.

As the distributed loadings were applied on the top deck by the steel blocks, cracking pattern on the concrete surface was checked after the loading stages finished when all the steel blocks removed from the deck. All the information obtained from the transducers and gauges were automatically recorded by a data acquisition system at intervals when each loading stage was stable during the tests.

3. Experimental results and discussion

3.1 Load-displacement relationship

The relationships between load and vertical displacements at mid-span (Sec.4~5,) and 1/4 span (Sec.3) of the girder are shown in Fig.5. The load is the self-weight of steel blocks applied on the deck of the girder. It can be found that the deflection increased almost linearly with the applied load at the beginning elastic stage, after the concrete in bottom steel tube cracked at the load about 1500kN, the flexural rigidity of the girder reduced leading to the deflection increased dramatically. The deflection at cantilever flange (Dy4-2, 3) were observed and compared with that at bottom slab (Dy4-1), as shown in Fig. 5. The deflections were almost the same at each loading step, which demonstrated that local deformation of cantilever flange was not occurred during all stages. In addition, the deflection variation along longitudinal direction under different loading levels is presented in Fig. 6, the deflection increased with the load and distributed symmetrically with respect to middle span.

The out-of-plane deformation of the web was measured by the lateral displacement gauge near the supporting section (Sec.2), the load-deformation relationship curves are described in Fig. 7. The out-of-plane deformation of the web increased almost linearly with the applied load, and no shear buckling appeared till ultimate state. As the load cannot be applied absolute symmetrically

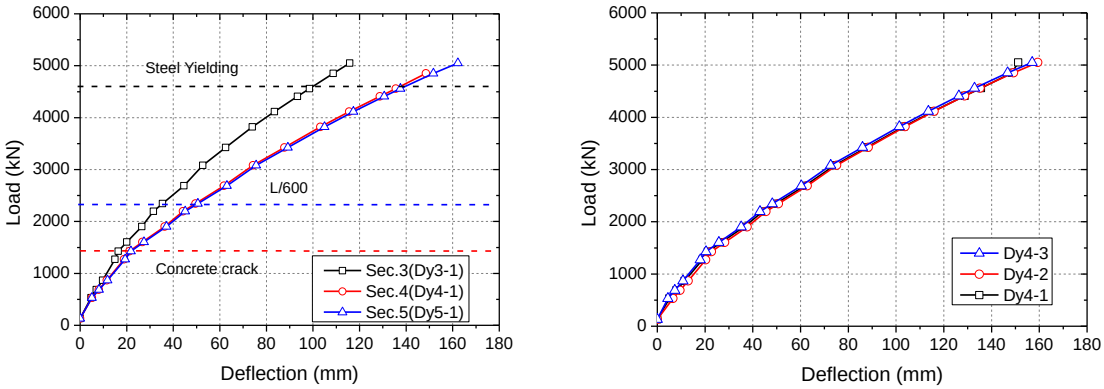

Fig. 5 Load-displacement relation

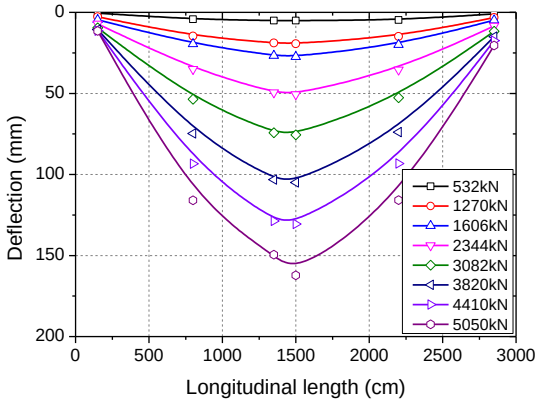

Fig. 6 Deflection along longitudinal direction of composite girder

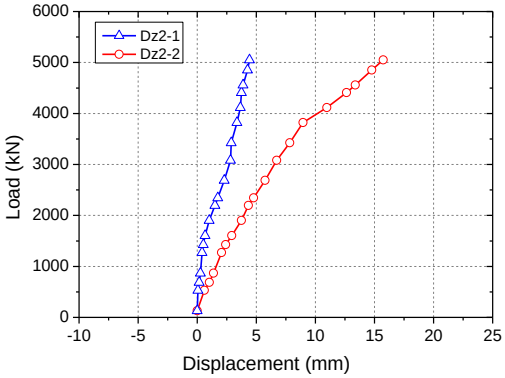

Fig. 7 Relation between load and out-of-plane displacement

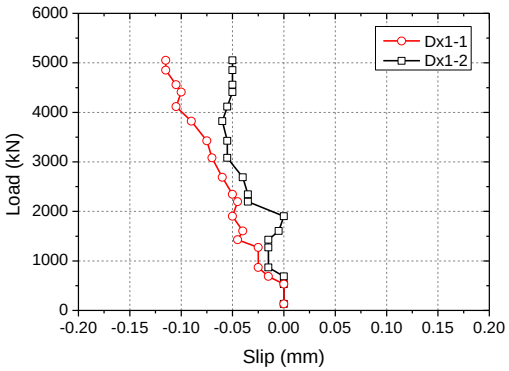

Fig. 8 Relation between load and slip at end section

on the deck in transverse direction, the value of out-of-plane deformation at both webs was different from each other.

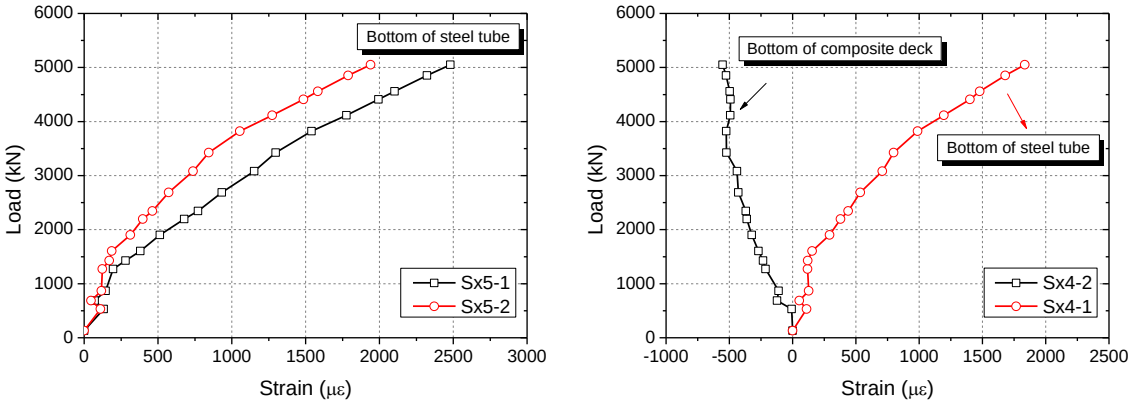

Fig. 9 Load-strain curves on steel plate

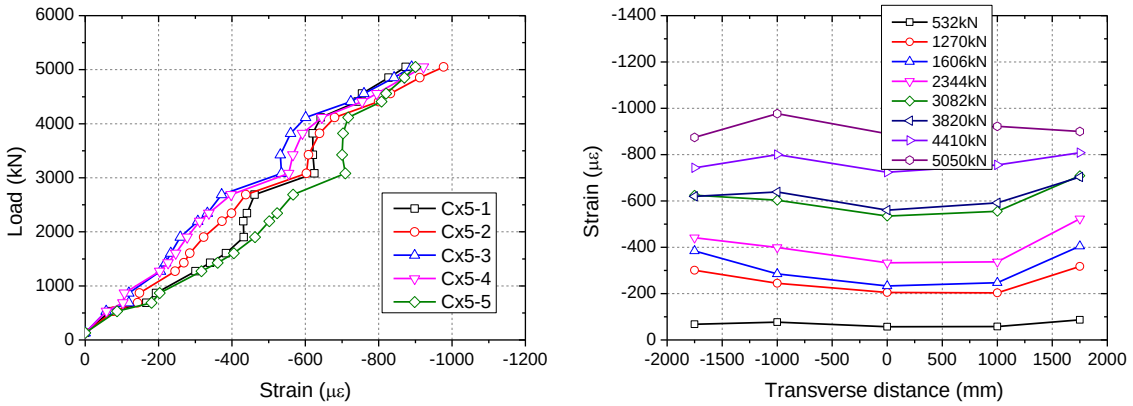

(a) Load-strain curves (b) Normal strain distribution

Fig. 10 Normal strain on concrete surface at section 5

The relative slip between concrete slab and steel plate at the end section (Sec.1) was obtained through the LTVDs (Dx1-1, 2), as shown in Fig. 8. The maximum slip at the ultimate load was about 0.1mm which denoted that concrete slab fully connected to the steel plate by the bent-up bars as shear connectors.

3.2 Strain results

3.2.1 Flexural strain

The normal strains on the bottom of steel tube and composite deck at the middle section are shown in Fig. 9. The normal strains on the bottom steel tube increased linearly in elastic stage, and the value was less than the tensile strain of infill concrete, which indicated that infill concrete resisted bending moment with steel tube together. When the strain reached the ultimate tensile value of infill concrete, the contribution of cracked concrete in tension to flexure strength was ignored, strain of steel plate increased rapidly till yielding of steel. On the other hand, the bottom steel plate of composite deck (Sx4-2) was compressed and the normal strain increased almost

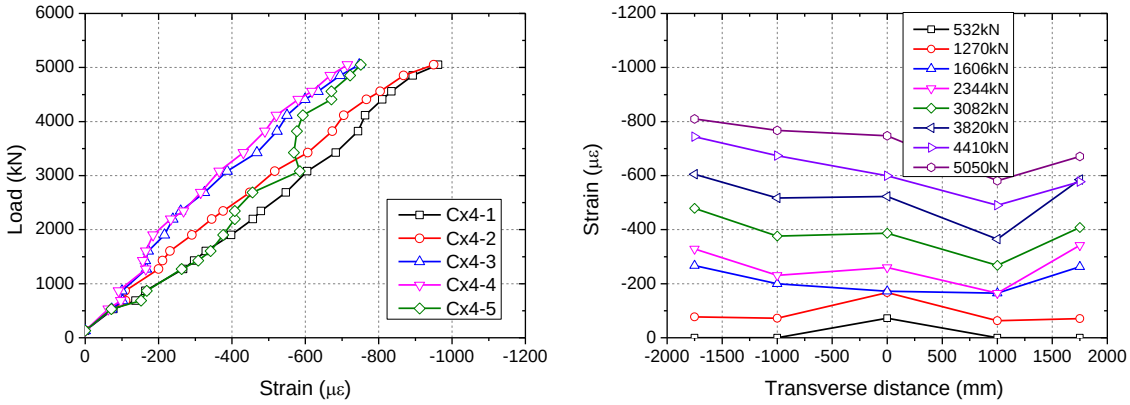

(a) Load-strain curves (b) Normal strain distribution

Fig. 11 Normal strain on concrete surface at section 4

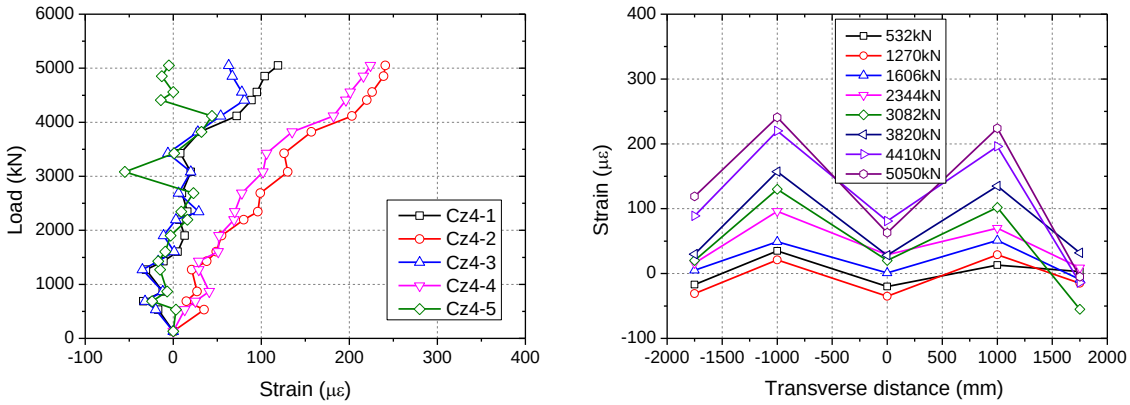

(a) Load-strain curves (b) Transverse strain distribution

Fig. 12 Transverse strain on concrete surface at section 4

linearly at all loading stages, and the value was much less than the yield strain.

The normal strains on the concrete surface of top composite deck at the middle sections are shown in Figs. 10 and 11. The normal strain increased almost linearly with the applied load, the strain distributed more uniformly at section 5 than that at section 4 in transverse direction due to the effect of diaphragm. The transverse strains on the concrete surface of top composite deck at section 4 are shown in Fig. 12. The transverse strains changed from compression to tension as load increased, and the maximum transverse strain appeared at the connection between corrugated steel webs and composite beck, the value is about 200$\mu\varepsilon$ at ultimate state.

3.2.2 Shear strain

The shear strains (γ) on the corrugate steel web are obtained according to measurement by strain rosette, as follows

$$\gamma = \varepsilon_x + \varepsilon_y - 2\varepsilon_{45^\circ} \tag{1}$$

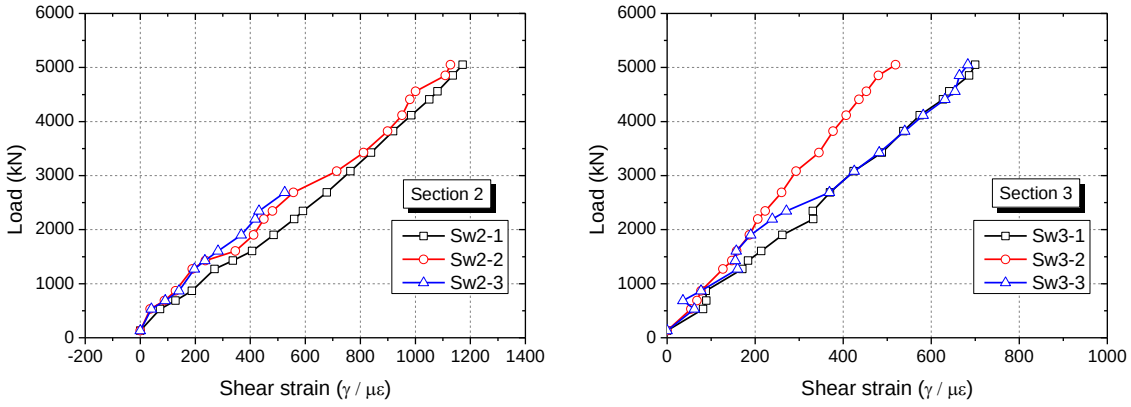

(a) Load-strain curves

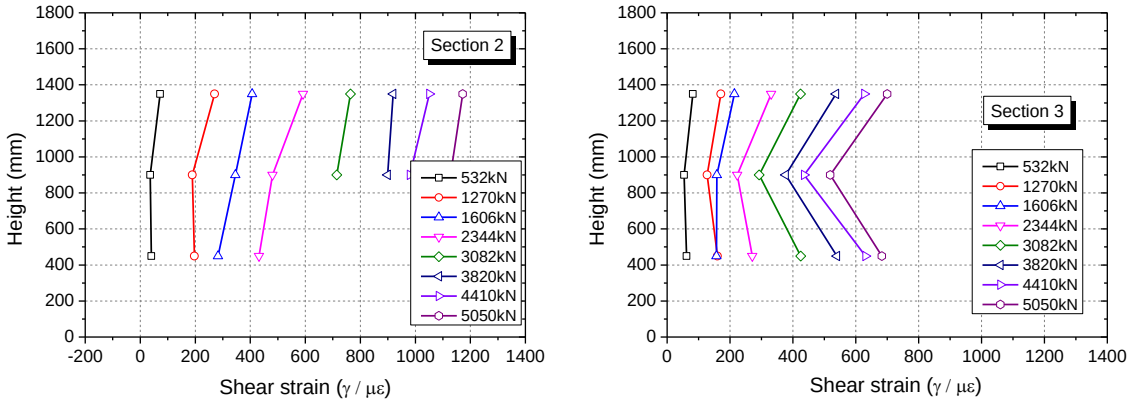

(b) Shear strain distribution along height of corrugated web

Fig. 13 Shear strain on corrugated steel web

where ε_x, ε_y and ε_{45° are the longitude, vertical and inclined strain respectively.

The shear strains of corrugate steel web near the end support section (Sec.2) and 1/4 span section (Sec.3) are shown in Fig. 13. It should be noted that gauge Sw2-3 was failed accidently after loading level of 2500 kN. The shear strains were in linear proportion to the applied load, and distributed almost uniformly along the height of web. The maximum shear strain of the web was much less than the yielding one, which indicated that the corrugated steel was still in elastic stage at the ultimate state of the test.

3.3 Load carrying capacity and neutral axis

Table 1 lists the test results of load carrying capacity and related stress level under different stages. In the table, the design load is determined according to the specification JTG D62-2004 (Ministry of communication of China 2004); while the serviceability state is defined as the maximum deflection reaches to L/600 (L is the span of girder). It can be found that the design load is much less than the concrete cracking load, which means the structure is in elastic state and the transformed section (composed of infill concrete steel tube, prestressing tendons and composite

Table 1 Test results at different loading stages

State	Load (kN)	Bending moment (kN.m)	Deflection (mm)	Concrete compressive stress (MPa)	Steel tensile stress (MPa)	Shear stress of web (MPa)
Design load	875	3281	11.8	4.0	30	15
Concrete cracking	1420	5218	21.8	7.1	56	27
serviceability state	2344	8614	50.0	9.8	155	47
Steel Yielding	4853	17834	151.7	18.2	412	85
Ultimate state	5050	18559	167.2	20.1	419	92

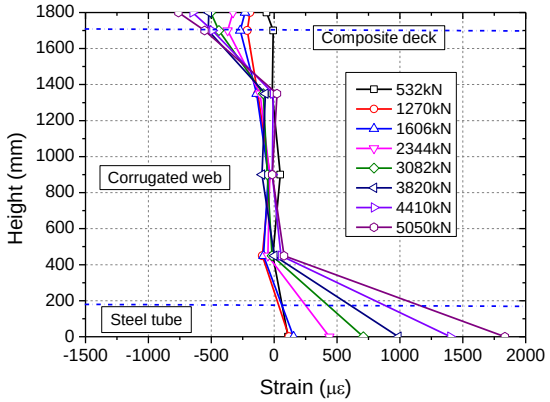

Fig. 14 Normal strain distribution along height at section 4

deck) can be used to calculate strain state. In addition, the normal stress of steel tube and shear stress of steel web are much less than the allowable values at the serviceability state. And the load at steel yielding is about 5.5 and 2 times to the design load and serviceability load respectively, while the defection at steel yielding is about 13 and 3 times to the deflection at design and serviceability state respectively. Moreover, after final stage of loading, all the steel blocks were removed to check the cracking or crushing of concrete on the surface, it was found that no visible concrete cracking and crushing on the deck. From the experimental results, it was confirmed that the composite girder with corrugated steel webs has enough load carrying capacity and ductility.

The normal strains at section 4 are depicted along the height of the girder, as shown in Fig. 14, in which the normal strains on the top and bottom slab are located at the center of the cross-section. It can be found that the normal strains on the corrugated web are very small even after the yielding of bottom slab, which verifies the "accordion effect" of corrugated web. Therefore, flexural strength is provided by the top and bottom slabs with almost no contribution from the corrugated webs.

The relation between load and neutral axis is shown in Fig. 15, in which neutral axis was calculated based on the strain distribution along the height of the girder at each loading step. It was revealed that the initial neutral axis of cross-section in elastic stage was almost the same as that of an un-cracked section. As the load increased, the neutral axis moved upward from the un-cracked section (elastic state) to plastic section (ultimate state).

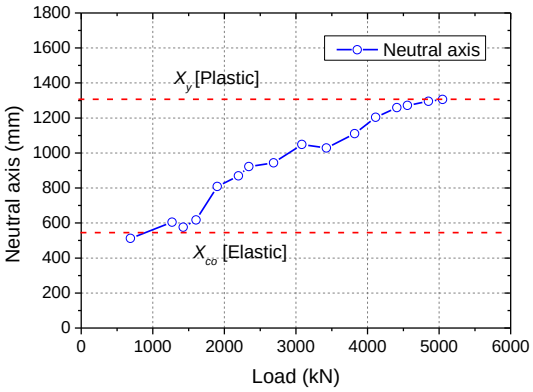

Fig. 15 Load-neutral axis relationship

4. Finite element analysis

4.1 Finite element model

The nonlinear finite element analysis (FEA) program ANSYS version 11.0 (2005) was used to model the load carrying capacity test of composite box-girder with corrugated webs accounting for material nonlinearity. Solid elements, shell elements, link elements were used to simulate the concrete deck, steel girder and prestressing tendons respectively. Perfect bonding between prestressing tendons and surrounded concrete was assumed. The specimens were subjected to uniform distributed load at corresponding position, and simply supported on the bearings, which was simulated the same as loading test.

For the concrete slab, an eight-node three dimensional (3D) reinforced concrete solid (SOLID65) element was used. The reinforcing bars in the concrete slab were assumed to be "smeared" throughout the solid elements with the volume ratios. The SOLID65 element is based on a constitutive model for the tri-axial behavior of concrete by the failure criterion of William and Warnke (1975). The element includes a smeared crack analogy for cracking in tension zones and a plasticity algorithm to account for the possibility of concrete crushing in compression. For concrete in compression, the uniaxial stress-strain relationship (Fig. 16) is obtained using the Hongnestad model and incorporated into the FE model with the Multi-linear Isotropic Hardening (MISO) option, the relationship between the stress (f_c) and strain (ε_c) of concrete in compression is assumed to be a parabolic curve for the strain under ε'_c and constant afterwards, as follows

$$f_c = f'_c\left[2\left(\frac{\varepsilon_c}{\varepsilon'_c}\right)-\left(\frac{\varepsilon_c}{\varepsilon'_c}\right)^2\right] \quad \varepsilon_c \le \varepsilon'_c$$

$$f_c = f'_c \quad \varepsilon'_c < \varepsilon_c \le \varepsilon_u \qquad (2a, b)$$

where f_c and ε_c are the compressive stress and strain of concrete, f'_c and ε'_c the compressive strength of concrete and the corresponding strain. The ultimate concrete strain ε_{cu} is set at 0.0033.

On the tensile side, linear model (Fig. 16) was adopted for the relation between stress (f_t) and strain (ε_t), and after crack resistance strength (f_{tr}), tensile stress reduced lineally to 0 at ultimate

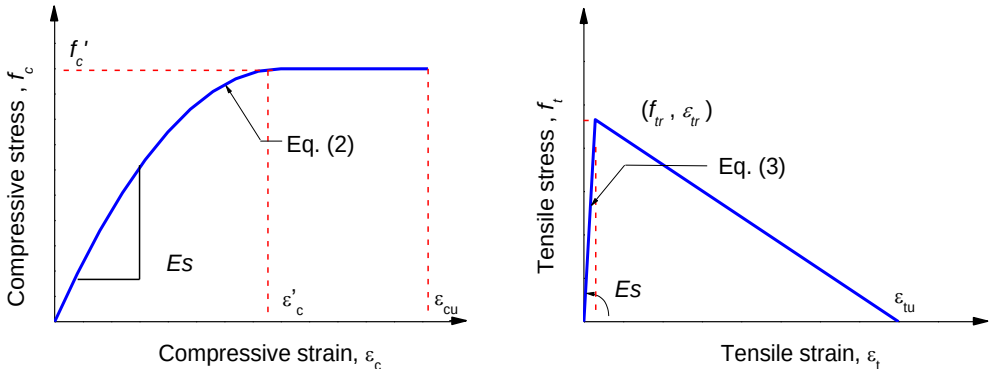

Fig. 16 Stress-strain relationship of concrete

strain ($\varepsilon_{tu}=f_{ry}/E_s$: f_{ry}, E_s are the yield stress and Young's modulus of rebar) considering the soften of concrete in tension, which are given by

$$f_t = E_c\varepsilon_t \le f_{tr} \quad \varepsilon_t \le \varepsilon_{tr}$$

$$f_t = f_{tr}\left(1-\frac{\varepsilon_t-\varepsilon_{tr}}{\varepsilon_{tu}-\varepsilon_{tr}}\right) \quad \varepsilon_{tr} < \varepsilon_t \le \varepsilon_{tu} \tag{3a, b, c}$$

$$f_{tr} = 0.23 f_c'^{2/3}$$

The corrugated steel webs and steel plates are simulated by an 8-node structural shell element SHELL93. The element has plasticity, stress stiffening, large deflection, and large strain capabilities. The stress-strain relationship of steel plate is taken as elastic-perfectly-plastic and incorporated into FE model with Bilinear Kinematic Hardening (BKIN) option. The assumed stress-strain curve is shown in Fig. 17, as following

$$\sigma_s = E_s\varepsilon_s \le \sigma_y \quad \varepsilon_s \le \varepsilon_y$$

$$\sigma_s = \sigma_y + \left(\sigma_u-\sigma_y\right)\frac{\varepsilon_s-\varepsilon_h}{\varepsilon_u-\varepsilon_h} \le \sigma_u \quad \varepsilon_y < \varepsilon_s \le \varepsilon_u \tag{4a, b}$$

where ε_s, σ_s are the strain and stress of steel, E_s is the Young's modulus of steel, σ_y and σ_u are the yield and ultimate strength of steel, respectively. In the elastic range, Young's modulus is 200 GPa and Poisson's ratio is 0.3. In the inelastic range, Von Mises yield criteria is used to define isotropic yielding.

The prestressed tendons are modeled by 3D two-node spar element LINK8. This element is a uniaxial tension-compression element with three degrees of freedom at each node. The stress-strain relationship of prestressed tendons is obtained from Ramberg-Osgood's equation (Eq. (5)) as shown in Fig. 18. The slip between prestressed tendons and concrete is ignored through sharing the nodes of SOLID65 element with those of LINK8 element. An initial strain is given in LINK8 element to simulate prestressing through real constant option.

$$f_{ps} = E_p\varepsilon_{ps} \le f_{py} \quad \varepsilon_{sp} \le \varepsilon_{py}$$

$$f_{ps} = E_p \varepsilon_{ps} \left[1 + \left(\frac{E_p \varepsilon_{ps}}{f_{pu}} \right)^R \right]^{-\frac{1}{R}} \leq f_{pu} \qquad \varepsilon_s > \varepsilon_{py} \tag{5a, b}$$

where ε_{ps}, f_{ps} are the strain and stress of prestressed tendon, E_p is Young's modulus of prestressed tendon, f_{py} and f_{pu} are the yield and ultimate strength of prestressed tendon respectively, R is taken as 4.38 in general.

The finite element model of composite box-girder with corrugated webs is shown in Fig.19. The Newton-Raphson iterative procedure was used to solve the nonlinearity by continuously updating the element stiffness matrix. Load steps were specified to determine ultimate load. At the end of each step, the program adjusted the stiffness matrix to reflect the nonlinear changes in stiffness of the structure.

4.2 Finite element analysis results

The load-displacement curves at middle section and 1/4 span section obtained from numerical simulation were compared to that obtained from the loading test, as shown in Fig. 20. It is found that in the linear region, the load displacement curves from numerical studies agree well with the

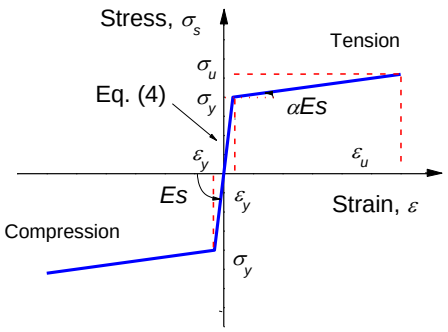

Fig. 17 Stress-strain relationship of steel plate

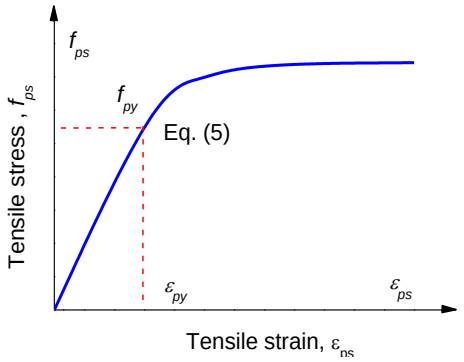

Fig. 18 Stress-strain relationship of prestressed tendon

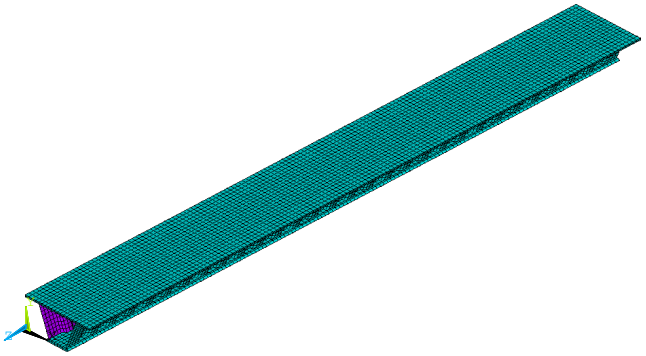

Fig. 19 Finite element model

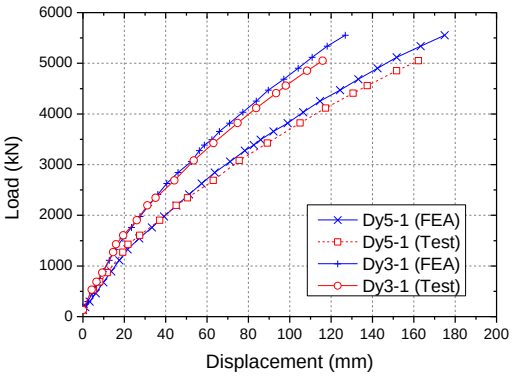

Fig. 20 Load-displacement curves from test and FEA

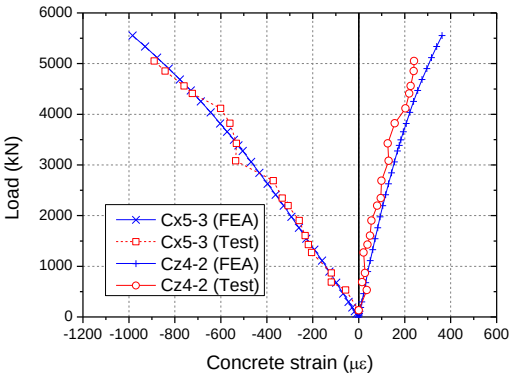

(a) Load-strain curves

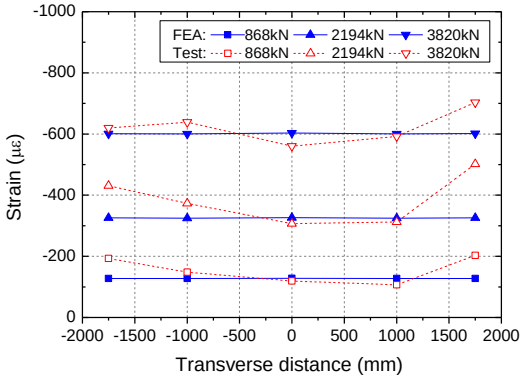

(b) Normal strain distribution

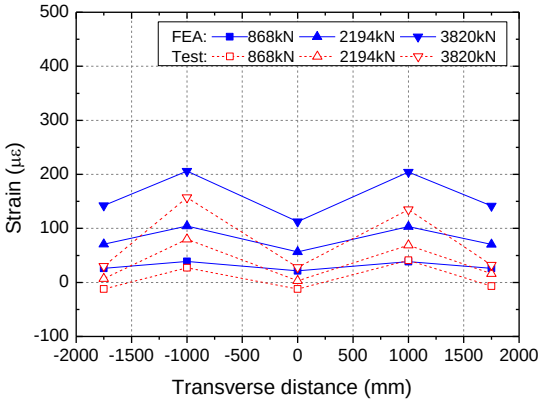

(c) Transverse strain distribution

Fig. 21 Concrete strain results obtained from test and FEA

measured results. However, in the nonlinear region after girder yielding, the rigidity of FE model is slightly stronger than that of the test girder. This is presumably because the residual stress is not considered, moreover perfect material constitutive relationship and boundary condition are

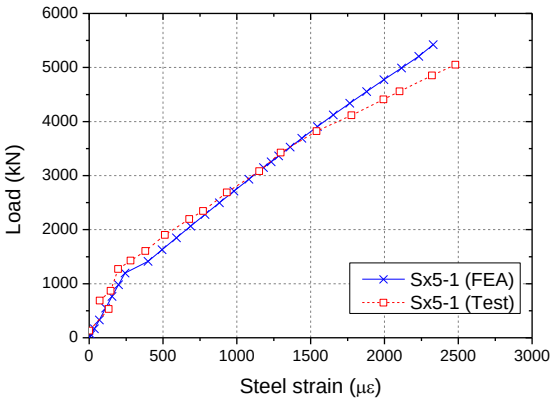

Fig. 22 Load-strain curves for steel tube obtained from test and FEA

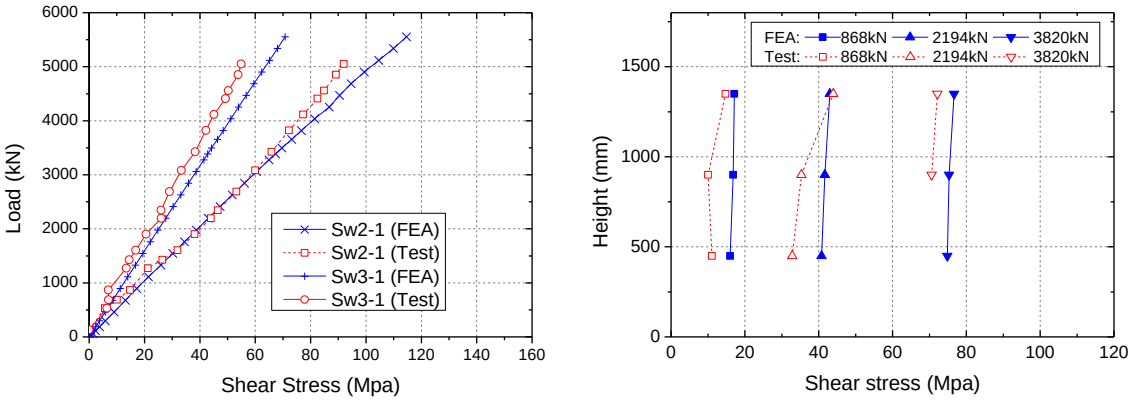

(a) Load-stress curves (b) Shear stress distribution along the height of web

Fig. 23 Comparison of experimental and numerical shear stress of corrugated steel web

assumed in the finite element analysis, which may result in slightly larger stiffness of FE model than that of the test girder.

The tested normal and transverse strains on the concrete deck at middle span (Sec.4~5) were observed and compared to the numerical ones, and the compared load-strain curves and strain distribution along the width of deck are shown in Fig. 21. Additionally, the normal strain on the bottom steel tube at middle section was obtained from the experimental and numerical results, as shown in Fig. 22. The comparison results of steel and concrete normal strains indicate that numerical flexural strains agree well with the tested ones. And the numerical normal strains distributed more uniformly in transverse direction than tested one, because the tested load could not be applied uniformly as the simulated one.

The experimental shear stress of corrugated steel web was calculated form the measured shear strain and shear module, then compared to the results from finite element analysis. The compared load-stress curves and stress distribution along the height of web are shown in Fig. 23. It was observed that the numerical and tested shear stress increased linearly with the applied load, and the load-stress curves from test and FEA coincided with each other. However, the shear stress from

the numerical simulation are slightly larger than that from experimental result, which might be the shear resistance ensured by the diaphragm were not considered in the finite element analysis.

5. Simplified analytical method

5.1 Bending strength

According to previous studies (He *et al.*2012c, Mo *et al.* 2003) and test results, it can be found that flexural strength of composite girders with a corrugated steel webs is provided by the top and bottom slabs without considering the contribution of corrugated webs due to its "accordion effect". Furthermore, there is no interaction between flexure and shear behavior for such kind girders. Thus, the ultimate flexural capacity of composite girders with corrugated steel webs can be based on the strength of top and bottom slabs. On the basis of experimental results of the fabricated composite box girder with corrugated webs, some assumptions are proposed for analytical model to predict bending moment:

(1) Concrete are fully connected to steel plate for both composite deck and steel tube, and the strain of slabs changes lineally along the height satisfying supposed plane-section (only slabs without corrugated webs in section) assumption.

(2) The applied load in experiment is assumed uniformly distributed on the deck, the bending moment at middle section (M_q) can be calculated as M_q=W_q×L/8, in which W_q is the total applied load (kN), L is the span of the girder.

(3) The non-linear model is adopted for the relationship between the stress (f_c) and strain (ε_c) of concrete in compression, which is assumed to be a parabolic curve for the strain under ε'_c and constant afterwards, as shown in Eq. (2). On the tensile side, linear model is adopted for the relationship between the stress and strain. After crack resistance strength (f_{tr}), the contribution of cracked concrete in tension to flexure strength is ignored.

(4) Elastic-perfectly plastic model is used for steel and prestressed tendon, and linear model is adopted for the relationship between the stress and strain up to the yield stress, however strain hardening effect is not considered for safety reason.

A simplified analytical method has been proposed to calculate the bending strength of composite girder with corrugated steel webs using a multiple layers model. Only the top and bottom slabs are considered in the cross-section to resist bending moment. During the construction and loading process, four analytical stages are considered, including: (a) pre-tension before concrete casting on the top deck; (b) concrete cracking in bottom slab; (c) yielding of steel tube; (d) ultimate state caused by plastic cross-section. The details of calculation for each stage are presented as follows:

(a) Stage 1: Pre-tension before concrete casting

The box girder was pre-tensioned on the prestressing pedestal, and the prestressing released after the strength of infill concrete reached more than 80% of hate design compressive strength. The pre-tension force was applied to a transformed section (composed of infill concrete steel tube, prestressing tendons and steel plates). Then, the box girder was supported on the bearings, and concrete was poured on the top deck. The moment caused by self-weight of the girder (M_g) is applied at the transformed section. Fig. 24 shows the strain and stress distribution of the cross-section.

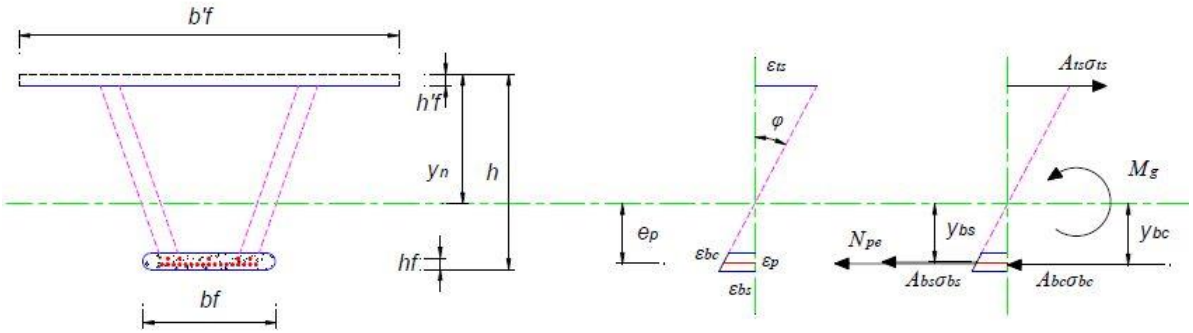

(a) Section (b) Strain (c) Stress & Force

Fig. 24 Section analysis under stage 1: pre-tension before concrete casting

The section analysis at this stage includes the response of the prestressing force N_{p0} and the moment M_g, the stress and strain of infill concrete $\sigma_{bc,0}$, $\varepsilon_{bc,0}$ and stress and strain of steel tube $\sigma_{bs,0}$, $\varepsilon_{bs,0}$ are calculated as

$$\varepsilon_{bc,0}=\frac{1}{E_s}\left(\frac{N_{pe}}{A_0}+\frac{N_{pe}e_p}{I_0}y_{bc,0}-\frac{M_g}{I_0}y_{bc,0}\right);\quad \sigma_{bc,0}=E_c\varepsilon_{bc,0}$$
$$\varepsilon_{bs,0}=\frac{1}{E_s}\left(\frac{N_{pe}}{A_0}+\frac{N_{pe}e_p}{I_0}y_{bs,0}-\frac{M_g}{I_0}y_{bs,0}\right);\quad \sigma_{bs,0}=E_s\varepsilon_{bs,0} \tag{6a~d}$$

where E_c, E_s are the Young's modulus of concrete and steel; A_0, I_0 are the area and moment of inertia for transformed section; e_p is the distance from the prestressing tendon to the neutral axis; $y_{bc,0}$, $y_{bs,0}$ are the distance from the calculated layer of bottom concrete and steel to the neutral axis respectively; N_{pe} is the applied prestressing force; y_n is the distance from top deck to the neutral axis.

(b) Stage 2: Concrete cracking

When the concrete stress reached the tensile strength f_t under bending moment M_{cr}, the initial crack occurred, and the strain $\varepsilon_{bc,cr}$ and stress $\sigma_{bc,cr}$ at the edge of tensile part are as follows

$$\varepsilon_{bc,cr}=\varepsilon_{bc,0}+\varepsilon_{cr};\quad \sigma_{bc,cr}=\sigma_{bc,0}+f_t \tag{7a, b}$$

where ε_{cr} is the crack strain when stress reached the tensile strength f_t.

The strain and stress distribution of the cross section under crack moment M_{cr} are shown in Fig. 25, the curvature Φ_{cr} at initial crack state can be obtained as

$$\phi_{cr}=\frac{\varepsilon_{bs}}{h-y_{cr}}=\frac{\varepsilon_{tc}}{y_{cr}} \tag{8}$$

where ε_{tc} is the concrete strain at top deck; y_{cr} is the distance from cracked neutral axis to the top deck, as shown in Fig. 25.

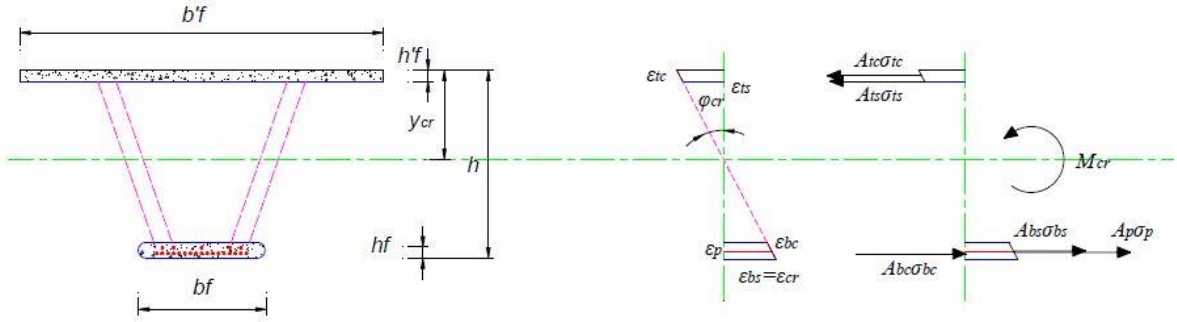

(a) Section (b) Strain (c) Stress & Force

Fig. 25 Section analysis under stage 2: Cracking of concrete

On the basis of strain-stress relation and deformation compatibility conditions, the compressive force C and the distance from the action point to the edge of compressive concrete y_c are expressed as

$$C = f_c b \int_{y_{cr}-h_f'}^{y_{cr}} \left(2\frac{\varepsilon_c}{\varepsilon_0} - \frac{\varepsilon_c^2}{\varepsilon_0^2}\right) dy; \quad y_c = y_{cr} - \frac{f_c b \int_{y_{cr}-h_f'}^{y_{cr}} \left(2\frac{\varepsilon_c}{\varepsilon_0} - \frac{\varepsilon_c^2}{\varepsilon_0^2}\right) y dy}{f_c b \int_{y_{cr}-h_f'}^{y_{cr}} \left(2\frac{\varepsilon_c}{\varepsilon_0} - \frac{\varepsilon_c^2}{\varepsilon_0^2}\right) dy} \tag{9a, b}$$

As the height of concrete in compressive zone $h'_f=h/18$, the distance from the action point to the edge of compressive concrete y_c can be assumed to be $0.5h'_f$ for simplification.

The tensile strain caused by external bending moment composed of two parts, one is the decompression strain, and the other is the tensile strain. According to the strain-stress relation, stress distribution of tensile concrete, and equilibrium conditions of bending moment $\sum M=0$ and axial force $\sum F=0$, the crack bending moment M_{cr} is given by

$$M_{cr} = \left[\sigma_{bc} A_c + \sigma_{bs} A_{bs} + \sigma_p A_p\right]\left(h - h_f' - h_f / 2\right) \tag{10}$$

where σ_{bc} , A_c are the stress and area of tensile concrete; σ_s, A_s are the stress and area of steel tube; σ_p , A_p are the stress and area of prestressed tendon; h_f is the height of steel tube.

(c) Stage 3: Yielding of steel tube

Once the crack resistance strength (f_t) of concrete is attained, the contribution of cracked concrete in tension to flexure strength is assumed to be ignored. When the tensile stress of steel tube approaches to yield stress (f_y), the strain $\varepsilon_{bs,y}$ and stress $\sigma_{bs,y}$ of steel plate in tension under the external bending moment M_y are given:

$$\varepsilon_{bs,y} = \varepsilon_{bs,0} + \varepsilon_y; \quad \sigma_{bs,y} = \sigma_{bs,0} + f_y \tag{11a, b}$$

where ε_y is the yield strain of steel.

The strains and stress distribution of the cross section under yielding moment M_y are shown in Fig. 26, the curvature Φ_y at steel tube yielding can be obtained as

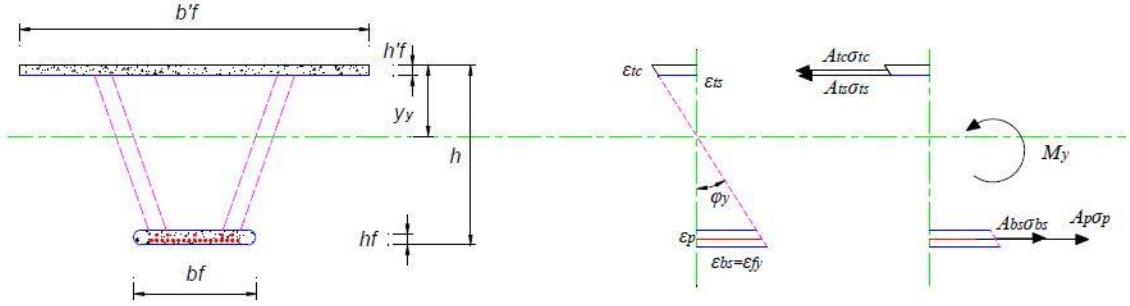

(a) Section (b) Strain (c) Stress & Force

Fig. 26 Section analysis under stage 3: Yielding of steel tube

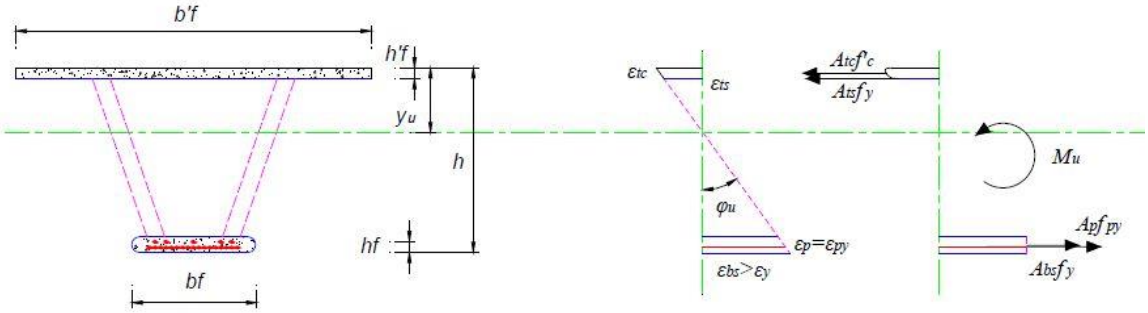

(a) Section (b) Strain (c) Stress & Force

Fig. 27 Section analysis under Stage 4: Ultimate state

$$\phi_y = \frac{\varepsilon_{bs}}{h - y_y} = \frac{\varepsilon_{tc}}{y_y} \tag{12}$$

where ε_{tc} is the concrete strain on top deck; ε_{bs} is the strain of steel tube; y_y is the distance from yield neutral axis to the top deck, as shown in Fig. 26.

Based on the strain-stress relation, stress distribution of tensile concrete, and equilibrium conditions of bending moment $\sum M=0$ and axial force $\sum F=0$, the yield bending moment M_y is given by

$$M_y = \left[\sigma_{bs} A_{bs} + \sigma_p A_p\right]\left(h - h_f^{'}/2 - h_f/2\right) \tag{13}$$

where σ_s , A_s are the stress and area of steel tube; σ_p , A_p are the stress and area of prestressed tendon; h_f is the height of steel tube.

(d) Stage 4: Ultimate state

The ultimate state is defined as the yield stress of steel tube (f_y) and prestressing tendon (f_{py}) are attained, and the compressive concrete stress reaches to maximum strength (f'_c). The ultimate bending moment M_u is calculated based on full plastic section, the strain and stress distribution is shown in Fig. 27.

Table 2 Comparison of test, FEA and simplified analytical results

State	Load (kN)			Concrete compressive stress (MPa)			Steel tensile stress (MPa)			Shear stress of web (MPa)		
	Ana.	Test	FEA	Ana.	Test	FEA	Ana.	Test	FEA	Ana.	Test	FEA
Concrete cracking	1131	1420	1320	5.35	7.1	6.3	14.9	14	15.1	28	27	26
Steel Yielding	4231	4558	4686	21.41	18.2	18.6	410	412	399	105	85	95
Ultimate state	4982	5050	5553	24.97	20.1	22.2	410	419	416	124	92	115

$$M_u = (A_p f_{py} + A_{bs} f_y)(h - h_f / 2 - h_f^{'} / 2) - M_g \tag{14}$$

5.2 Shear strength

The vertical shear force (V_x) assumed to be resisted by corrugated webs neglecting the contribution of top and bottom slabs, which is conservative in safety side for the design of corrugated webs. Moreover, the shear strength of composite girder is controlled by shear buckling or yielding of the corrugated web, generally the corrugated web should be designed to avoid buckling before steel yielding. The shear stress (τ) distributed almost uniformly and can be evaluate treating as a constant over the height as follows

$$\tau = \frac{V_x}{h_w t_w};\ V_x = \frac{W_q}{2} - \frac{W_q}{L} x \tag{15}$$

where h_w and t_w are the vertical height and thickness of corrugated steel webs; W_q is the total applied load; L is the span of the girder, x is the distance from the calculated section to the supporting end.

5.3 Simplified analytical results and discussion

On the basis of strain-stress relation, stress distribution of cross-section, and equilibrium conditions of bending moment and axial force, the bending moment and the stress of each component under different stages from simplified analytical method were obtained. The simplified analytical results (Ana.) were compared to test and FEA results, as shown in Table 2, where the concrete compressive stress is obtained at the center of top deck, the steel tensile stress is given at the center of bottom slab, shear stress of corrugated web is located near support section (Sec. 2). The load carrying capacity from test result was compared with that from simplified analysis and finite element simulation (Fig. 28), it can be seen that the simplified analytical load resistances at different stages are slightly less than test results (about 10%) and numerical results (about 11%), which indicates that the proposed simplified analytical method can be used to predict the load carrying capacity of such composite girder with corrugated steel webs in safety margin. In addition, the ratios of simulated results for load and stress to tested ones are 1.01 and 1.04 respectively, which demonstrates the accuracy of the proposed FE model. The tensile stress on the bottom of steel tube from simplified analytical results agreed well with those from the test and FE simulation. However, the shear stress of web near the support section obtained from the simplified

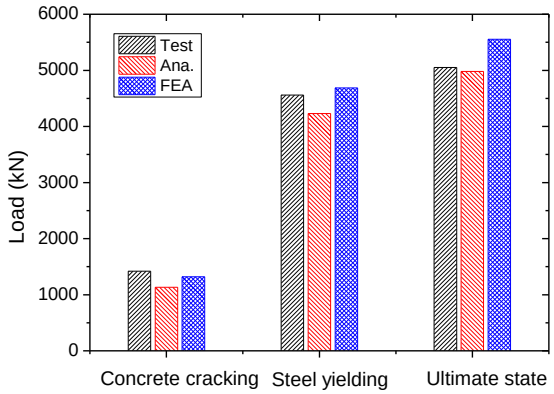

Fig. 28 Comparison of load carrying capacity at different stages

analysis is slight larger than those from test and FE simulation, it can be explained that the vertical shear load was assumed to be resisted only by the steel web in the simplified analysis, actually the top and bottom slabs accounts for part of the vertical shear load in test and FE simulation. Moreover, the compressive stress of concrete at top deck calculated by simplified analytical method is larger than those from test and FE simulation, due to the non-uniform distribution of concrete stress and the contribution of reinforcing bars at top deck are not considered in the simplified analytical method.

6. Conclusions

The mechanical performance of composite box girder with corrugated webs and steel tube slab has been experimentally investigated through full-scale model test. On the basis of experimental results, finite element model and simplified analytical method were proposed to evaluate the load carrying capacity. The following conclusions can be drawn from the present study:

• The model test results show that the structure is in elastic state under design load, and the normal stress of steel tube and shear stress of corrugated steel web are much less than the allowable values at serviceability state. Moreover, the load of steel yielding is about 5.5 and 2 times to the design load and serviceability load, while the defection at steel yielding is about 13 and 3 times to that at design and serviceability state respectively. Therefore, it is confirmed that the tested composite girder has enough loading capacity and ductility.

• A three dimensional finite element model taking material nonlinearity into consideration was established to investigate the static behavior under partially-uniform distributed load. The load-displacement curves and stress distribution predicted by FE model agree well with those obtained from experiment results, which demonstrates the accuracy of proposed FE model.

• The experimental and numerical normal strains on the corrugated web were very small even after the yielding of bottom slab, while the shear stress on the corrugated web increased linearly with the applied load and distributed uniformly along the height of steel web. It was revealed that flexural strength was resisted by the top and bottom slabs without considering the contribution of corrugated web due to its “accordion effect”, but shear force was almost resisted by corrugated web.

• Simplified analytical method of loading capacity prediction for composite girders with corrugated webs was proposed according to strain-stress relation, stress distribution of cross-section, and equilibrium conditions. Simplified analytical load resistance is slightly less than tested and numerical ones, which indicates that simplified analysis method can be used to predict the loading capacity of such composite girder with corrugated steel webs in safety margin.

Acknowledgments

The research described in this paper is financially supported by National Nature Science Foundation of China under Grant No. 51308070 and Ministry of transport of China under Grant No. 2013318822370. These supports are gratefully acknowledged. The assistance of experimental works from Xingtai Road & Bridge Construction Corporation and Tongji Univerisy are also appreciated.

References

ANSYS Release11.0. (2005), *ANSYS University Advanced*, ANSYS Inc.

Ayyub, B.M., Sohn, Y.G. and Saadatmanesh, H. (1992a), "Prestressed composite girders. I: experimental study for negative moment." *Journal of Structural Engineering, ASCE*, **118**(10), 2743-2762.

Ayyub, B.M., Sohn, Y.G. and Saadatmanesh, H. (1992b), "Prestressed composite girders. II: analytical study for negative moment", *J. Struct. Eng., ASCE*, **118**(10), 2763-2783.

Brozzetti, J. (2000), "Design development of steel-concrete composite bridges in France", *J. Construct. Steel Res.*, **55**(1-3), 229-243.

Chen, S. and Gu, P. (2005), "Load carrying capacity of composite beams prestressed with external tendons under positive moment." *Journal of Constructional Steel Research*, **61**(4), 515-530.

Cheyrezy, M., and Combault, J. (1990), "Composite Bridges with Corrugated steel Webs- Achievements and Prospects", *Proceedings, IABSE Symposium, Brussels, Mixed Structures and New Materials*, 479-484.

He, J., Liu, Y., Chen, A. and Yoda, T. (2012a), "Shear behavior of partially encased composite I-girder with corrugated steel web: Experimental study", *J. Construct. Steel Res.*, **77**, 193-209.

He, J., Liu, Y., Lin, Z., Chen, A. and Yoda, T. (2012b), "Shear behavior of partially encased composite I-girder with corrugated steel web: Numerical study", *J. Construct. Steel Res.*, **79**, 166-182.

He, J., Liu, Y., Chen, A. and Yoda, T. (2012c), "Mechanical behavior and analysis of composite bridges with corrugated steel webs: State-of-the-art", *Int. J. Steel Struct.*, **12**(3), 321-338.

He, J., Liu, Y., Chen, A., Wang, D. and Yoda, T. (2014), "Bending behavior of concrete-encased composite I-girder with corrugated steel web", *Thin Wall. Struct.*, **74**, 70-84.

Ibrahim, S.A., El-Dakhakhni, W.W. and Elgaaly, M. (2006), "Fatigue of corrugated-web plate girders: Experimental study", *J. Struct. Eng., ASCE*, **132**(9), 1371-1380.

Kosa, K., Awane, S., Uchino, H. and Fujibayashi, K. (2006), "Ultimate behavior of prestressed concrete bridge with corrugated steel webs using embedded connection", *J. Jap. Soc. Civil Eng., JSCE*, **62**, 202-220. (in Japanese)

Ministry of communication of China (2004), *Code for design of highway reinforced concrete and prestressed concrete bridges and culverts- JTG D62-2004*, China Communications Press, Beijing. (in Chinese)

Mo, Y.L. and Fan, Y. (2006), "Torsional design of hybrid concrete box girders", *J. Bridge Eng., ASCE*, **11**(3), 329-339.

Mo, Y.L., Jeng, C.H. and Krawinkler, H. (2003), "Experimental and analytical studies of innovative

prestressed concrete box-girder bridges", *Mater. Struct.*, **36**(2), 99-107.
Nakamura, S., Momiyama, Y., Hosaka, T. and Homma, K. (2002), "New technologies of steel/concrete composite bridges", *J. Construct. Steel Res.*, **58**(1), 99-130.
Sause, R., Abbas, H.H., Driver, R.G., Anami, K. and Fisher, J.W. (2006), "Fatigue life of girders with trapezoidal corrugated webs", *J. Struct. Eng., ASCE*, **132**(7), 1070-1078.
Sause, R. and Braxtan, T.N. (2011), "Shear strength of trapezoidal corrugated steel webs", *J.Construct. Steel Res.*, **67**(2), 223-236.
Willam, K.J. and Warnke, E.D. (1975), "Constitutive model for the triaxial behavior of concrete", *Proceedings of the International Association for Bridge and Structural Engineering*, ISMES, Bergamo, Italy.